

An Investigation of $D^+ \rightarrow \tau^+ \nu$

P. Rubin,¹ C. Cawfield,² B. I. Eisenstein,² I. Karliner,² D. Kim,² N. Lowrey,² P. Naik,²
C. Sedlack,² M. Selen,² E. J. White,² J. Wiss,² M. R. Shepherd,³ D. Besson,⁴
T. K. Pedlar,⁵ D. Cronin-Hennessy,⁶ K. Y. Gao,⁶ D. T. Gong,⁶ J. Hietala,⁶ Y. Kubota,⁶
T. Klein,⁶ B. W. Lang,⁶ R. Poling,⁶ A. W. Scott,⁶ A. Smith,⁶ S. Dobbs,⁷ Z. Metreveli,⁷
K. K. Seth,⁷ A. Tomaradze,⁷ P. Zweber,⁷ J. Ernst,⁸ H. Severini,⁹ S. A. Dytman,¹⁰
W. Love,¹⁰ V. Savinov,¹⁰ O. Aquines,¹¹ Z. Li,¹¹ A. Lopez,¹¹ S. Mehrabyan,¹¹ H. Mendez,¹¹
J. Ramirez,¹¹ G. S. Huang,¹² D. H. Miller,¹² V. Pavlunin,¹² B. Sanghi,¹² I. P. J. Shipsey,¹²
B. Xin,¹² G. S. Adams,¹³ M. Anderson,¹³ J. P. Cummings,¹³ I. Danko,¹³ J. Napolitano,¹³
Q. He,¹⁴ J. Insler,¹⁴ H. Muramatsu,¹⁴ C. S. Park,¹⁴ E. H. Thorndike,¹⁴ T. E. Coan,¹⁵
Y. S. Gao,¹⁵ F. Liu,¹⁵ M. Artuso,¹⁶ S. Blusk,¹⁶ J. Butt,¹⁶ J. Li,¹⁶ N. Menaa,¹⁶
R. Mountain,¹⁶ S. Nisar,¹⁶ K. Randrianarivony,¹⁶ R. Redjimi,¹⁶ R. Sia,¹⁶ T. Skwarnicki,¹⁶
S. Stone,¹⁶ J. C. Wang,¹⁶ K. Zhang,¹⁶ S. E. Csorna,¹⁷ G. Bonvicini,¹⁸ D. Cinabro,¹⁸
M. Dubrovin,¹⁸ A. Lincoln,¹⁸ D. M. Asner,¹⁹ K. W. Edwards,¹⁹ R. A. Briere,²⁰ I. Brock,²⁰
J. Chen,²⁰ T. Ferguson,²⁰ G. Tatishvili,²⁰ H. Vogel,²⁰ M. E. Watkins,²⁰ J. L. Rosner,²¹
N. E. Adam,²² J. P. Alexander,²² K. Berkelman,²² D. G. Cassel,²² J. E. Duboscq,²²
K. M. Ecklund,²² R. Ehrlich,²² L. Fields,²² L. Gibbons,²² R. Gray,²² S. W. Gray,²²
D. L. Hartill,²² B. K. Heltsley,²² D. Hertz,²² C. D. Jones,²² J. Kandaswamy,²²
D. L. Kreinick,²² V. E. Kuznetsov,²² H. Mahlke-Krüger,²² T. O. Meyer,²²
P. U. E. Onyisi,²² J. R. Patterson,²² D. Peterson,²² J. Pivarski,²² D. Riley,²² A. Ryd,²²
A. J. Sadoff,²² H. Schwarthoff,²² X. Shi,²² S. Stroiney,²² W. M. Sun,²² T. Wilksen,²²
M. Weinberger,²² S. B. Athar,²³ R. Patel,²³ V. Potlia,²³ H. Stoeck,²³ and J. Yelton²³

(CLEO Collaboration)

¹*George Mason University, Fairfax, Virginia 22030*

²*University of Illinois, Urbana-Champaign, Illinois 61801*

³*Indiana University, Bloomington, Indiana 47405*

⁴*University of Kansas, Lawrence, Kansas 66045*

⁵*Luther College, Decorah, Iowa 52101*

⁶*University of Minnesota, Minneapolis, Minnesota 55455*

⁷*Northwestern University, Evanston, Illinois 60208*

⁸*State University of New York at Albany, Albany, New York 12222*

⁹*University of Oklahoma, Norman, Oklahoma 73019*

¹⁰*University of Pittsburgh, Pittsburgh, Pennsylvania 15260*

¹¹*University of Puerto Rico, Mayaguez, Puerto Rico 00681*

¹²*Purdue University, West Lafayette, Indiana 47907*

¹³*Rensselaer Polytechnic Institute, Troy, New York 12180*

¹⁴*University of Rochester, Rochester, New York 14627*

¹⁵*Southern Methodist University, Dallas, Texas 75275*

¹⁶*Syracuse University, Syracuse, New York 13244*

¹⁷*Vanderbilt University, Nashville, Tennessee 37235*

¹⁸*Wayne State University, Detroit, Michigan 48202*

¹⁹*Carleton University, Ottawa, Ontario, Canada K1S 5B6*

²⁰*Carnegie Mellon University, Pittsburgh, Pennsylvania 15213*

²¹*Enrico Fermi Institute, University of Chicago, Chicago, Illinois 60637*

²²*Cornell University, Ithaca, New York 14853*

²³*University of Florida, Gainesville, Florida 32611*

(Dated: April 21, 2006)

Abstract

We test whether or not the τ lepton manifests the same couplings as the μ lepton by investigating the relative decay rates in purely leptonic D^+ meson decays. Specifically, we place the first upper limit on the ratio $R = \Gamma(D^+ \rightarrow \tau^+\nu) / \Gamma(D^+ \rightarrow \mu^+\nu)$. We use 281 pb^{-1} of data accumulated at the $\psi(3770)$ resonance with the CLEO-c detector, to determine $\mathcal{B}(D^+ \rightarrow \tau^+\nu) < 2.1 \times 10^{-3}$ at 90% confidence level (C. L.). The ratio of R to the Standard Model expectation of 2.65 then is < 1.8 at 90% C. L., consistent with the prediction of lepton universality.

I. INTRODUCTION

The Standard Model decay diagram for $D^+ \rightarrow \ell^+ \nu$ is shown in Fig. 1. The decay rate is given by [1]

$$\Gamma(D^+ \rightarrow \ell^+ \nu) = \frac{G_F^2}{8\pi} f_{D^+}^2 m_\ell^2 M_{D^+} \left(1 - \frac{m_\ell^2}{M_{D^+}^2}\right)^2 |V_{cd}|^2 \quad , \quad (1)$$

where M_{D^+} is the D^+ mass, m_ℓ is the mass of the charged final state lepton, V_{cd} is a Cabibbo-Kobayashi-Maskawa matrix element with a value we take equal to 0.225 [2], and G_F is the Fermi coupling constant.

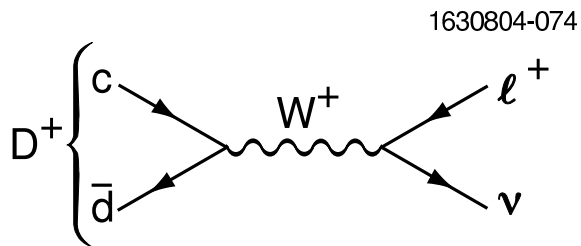


FIG. 1: The decay diagram for $D^+ \rightarrow \ell^+ \nu$.

The decay is helicity suppressed because the virtual W^+ is a spin-1 particle, and the final state consists of a naturally left-handed spin-1/2 neutrino and a naturally right-handed spin-1/2 anti-lepton that have equal energies and opposite momenta. The ratio of decay rates for any two different leptons is then fixed by well-known masses. For example, for $\tau^+ \nu$ to $\mu^+ \nu$, the expected ratio is

$$R \equiv \frac{\Gamma(D^+ \rightarrow \tau^+ \nu)}{\Gamma(D^+ \rightarrow \mu^+ \nu)} = \frac{m_{\tau^+}^2 \left(1 - \frac{m_{\tau^+}^2}{M_{D^+}^2}\right)^2}{m_{\mu^+}^2 \left(1 - \frac{m_{\mu^+}^2}{M_{D^+}^2}\right)^2} \quad . \quad (2)$$

Any deviation from this formula would be a manifestation of physics beyond the Standard Model. This could occur if any other charged intermediate boson existed that coupled to leptons differently than mass-squared. Then the couplings would be different for muons and τ 's. This would be a manifest violation of lepton universality, which has identical couplings of the muon, the tau, and the electron to the gauge bosons (γ , Z^0 and W^\pm) [3]. (We note that in some models of supersymmetry the charged Higgs boson couples as mass-squared to the leptons and therefore its presence would not cause a deviation from Eq. 2 [4].) Using measured masses [5], this expression yields a value of 2.65 with a negligibly small error.

We have already reported [6] $\mathcal{B}(D^+ \rightarrow \mu^+ \nu) = (4.40 \pm 0.66_{-0.12}^{+0.09}) \times 10^{-4}$, and established an upper limit of $\mathcal{B}(D^+ \rightarrow e^+ \nu) < 2.4 \times 10^{-5}$. It remains to measure or limit $\tau^+ \nu$, which is the subject of this paper. We note, for reference, that the predicted relative widths in the Standard Model are $2.65 : 1 : 2.3 \times 10^{-5}$ for the $\tau^+ \nu$, $\mu^+ \nu$ and $e^+ \nu$ final states, respectively.

The CLEO-c detector is equipped to measure the momenta and directions of charged particles, identify charged hadrons, detect photons and determine with good precision their

directions and energies. It has been described in more detail previously [7]. Particle identification is accomplished using both dE/dx information in the tracking drift chamber and in a separate Ring Imaging Cherenkov Detector (RICH) [8].

II. DATA SAMPLE AND SIGNAL SELECTION OVERVIEW

In this study we use 281 pb⁻¹ of CLEO-c data produced in e^+e^- collisions and recorded at the $\psi(3770)$ resonance. At this energy, the event sample consists of a mixture of pure D^+D^- , $D^0\bar{D}^0$, three-flavor continuum, and $\gamma\psi(2S)$ events. There are also $\tau^+\tau^-$ pairs, two-photon events, and non- $D\bar{D}$ decays of the $\psi(3770)$, whose production rates are small enough for them not to contribute background in this study.

This analysis follows very closely our previous study of $D^+ \rightarrow \mu^+\nu$ [6, 9]. First we fully reconstruct a sample of hadronic D^- decays, that we call tags, and then search for tracks that are consistent with a π^+ from the decay sequence $D^+ \rightarrow \tau^+\nu$, $\tau^+ \rightarrow \pi^+\bar{\nu}$, rather than a muon directly from two-body D decay. Besides using D^- tags and searching for $D^+ \rightarrow \tau^+\nu$, $\tau^+ \rightarrow \pi^+\bar{\nu}$ we also use the charge-conjugate D^+ tags and search for $D^- \rightarrow \tau^-\bar{\nu}$, $\tau^- \rightarrow \pi^-\nu$; in the rest of this paper we will not mention the charge-conjugate modes explicitly, but they are always used. The loss of rate compared to the muon case, caused by the $\mathcal{B}(\tau^+ \rightarrow \pi^+\nu)$ of $(11.06 \pm 0.11)\%$ [5], is somewhat compensated for by the larger $D^+ \rightarrow \tau^+\nu$ branching ratio as given by Eq. 1. This search has a smeared signal region as compared to the muon case because of the extra missing neutrino, and therefore backgrounds are a much more serious concern.

We examine all the recorded events and retain those containing at least one charged D candidate in the modes listed in Table I. Track selection, particle identification, π^0 , K_S and muon selection cuts are identical to those described in Ref. [9].

We have investigated using other τ decay modes but they all have significant problems. The semileptonic mode $e\nu\bar{\nu}$ is embedded in a large D^+ semileptonic background. The $\rho^+\bar{\nu}$ mode has a MM² resolution approximately twice as poor, and the $\pi^+\pi^+\pi^-\bar{\nu}$ mode has several additional associated backgrounds, for example $D^+ \rightarrow \pi^+\pi^+\pi^-\pi^0$ and $\eta\mu^+\nu$, that severely limit its usefulness.

III. RECONSTRUCTION OF CHARGED D TAGGING MODES

Tagging modes are fully reconstructed by first evaluating the difference in the energy, ΔE , of the decay products with the beam energy. We require the absolute value of this difference to contain 98.8% of the signal events, i.e. to be within approximately 2.5 times the r.m.s. width of the peak value. The r.m.s. widths vary from 7 MeV in the $K^+K^-\pi^-$ mode to 14 MeV in the $K^+\pi^-\pi^-\pi^0$ mode. For the selected events we then calculate the reconstructed D^- beam-constrained mass defined as

$$m_{\text{BC}} = \sqrt{E_{\text{beam}}^2 - \left(\sum_i \vec{p}_i\right)^2}, \quad (3)$$

where i runs over all the final state particles. The beam-constrained mass has better resolution than merely calculating the invariant mass of the decay products since the beam has a small energy spread.

The m_{BC} distributions for all D^- tagging modes considered in this data sample are shown in Fig. 2. They are listed in Table I, along with the numbers of signal events and background events within the regions shown by the arrows in Fig. 2. The tag candidates are subjected to ΔE and m_{BC} cuts explained in our previous paper [6]. The numbers of tagged events are determined from fits of the m_{BC} distributions to a signal function plus a background shape. For the background we fit with a shape function analogous to one first used by the ARGUS collaboration [10], that has approximately the correct threshold behavior at large m_{BC} . To use this function, we first fit it to the data selected by using ΔE sidebands, defined as $5\sigma < |\Delta E| < 7.5\sigma$, where σ is the r.m.s. width of the ΔE distribution. Doing this mode by mode and allowing the normalization to float, we fix the shape parameters. For the signal we use a lineshape similar to that used for extracting photon signals from electromagnetic calorimeters because of the tail towards high mass caused by initial-state radiation [11]. The functional form is

$$f(m_{\text{BC}}|m_D, \sigma_{m_{\text{BC}}}, \alpha, n) = \begin{cases} A \cdot \exp\left[-\frac{1}{2}\left(\frac{m_{\text{BC}}-m_D}{\sigma_{m_{\text{BC}}}}\right)^2\right] & \text{for } m_{\text{BC}} < m_D - \alpha \cdot \sigma_{m_{\text{BC}}} \\ A \cdot \frac{\left(\frac{n}{\alpha}\right)^n e^{-\frac{1}{2}\alpha^2}}{\left(\frac{m_{\text{BC}}-m_D}{\sigma_{m_{\text{BC}}}} + \frac{n}{\alpha} - \alpha\right)^n} & \text{for } m_{\text{BC}} > m_D - \alpha \cdot \sigma_{m_{\text{BC}}} \\ \text{here } A^{-1} \equiv \sigma_{m_{\text{BC}}} \cdot \left[\frac{n}{\alpha} \cdot \frac{1}{n-1} e^{-\frac{1}{2}\alpha^2} + \sqrt{\frac{\pi}{2}} \left(1 + \text{erf}\left(\frac{\alpha}{\sqrt{2}}\right)\right)\right] & \end{cases} \quad (4)$$

Here m_{BC} is the measured mass of each candidate, m_D is the “true” (or most likely) mass, $\sigma_{m_{\text{BC}}}$ is the mass resolution, and n and α are parameters governing the shape of the high mass tail. All these quantities are allowed to float in the separate fits of each mode.

| Mode | Signal | Background |
|----------------------|------------------|------------|
| $K^+\pi^-\pi^-$ | 77387 ± 281 | 1868 |
| $K^+\pi^-\pi^-\pi^0$ | 24850 ± 214 | 12825 |
| $K_S\pi^-$ | 11162 ± 136 | 514 |
| $K_S\pi^-\pi^-\pi^+$ | 18176 ± 255 | 8976 |
| $K_S\pi^-\pi^0$ | 20244 ± 170 | 5223 |
| $K^+K^-\pi^-$ | 6535 ± 95 | 1271 |
| Sum | 158354 ± 496 | 30677 |

TABLE I: Tagging modes and numbers of signal and background events determined from the fits shown in Fig. 2.

We use a total of $158,354 \pm 496 \pm 475$ single tag events for further analysis. The systematic error on this number is determined by varying the background function and is estimated at 0.5%.

IV. $D^+ \rightarrow \tau^+\nu$ SELECTION CRITERIA

As in our search for $D^+ \rightarrow \mu^+\nu$, we calculate the missing mass squared (MM^2) defined as

$$\text{MM}^2 = (E_{\text{beam}} - E_{\text{track}})^2 - (-\vec{p}_{D^+} - \vec{p}_{\text{track}})^2, \quad (5)$$

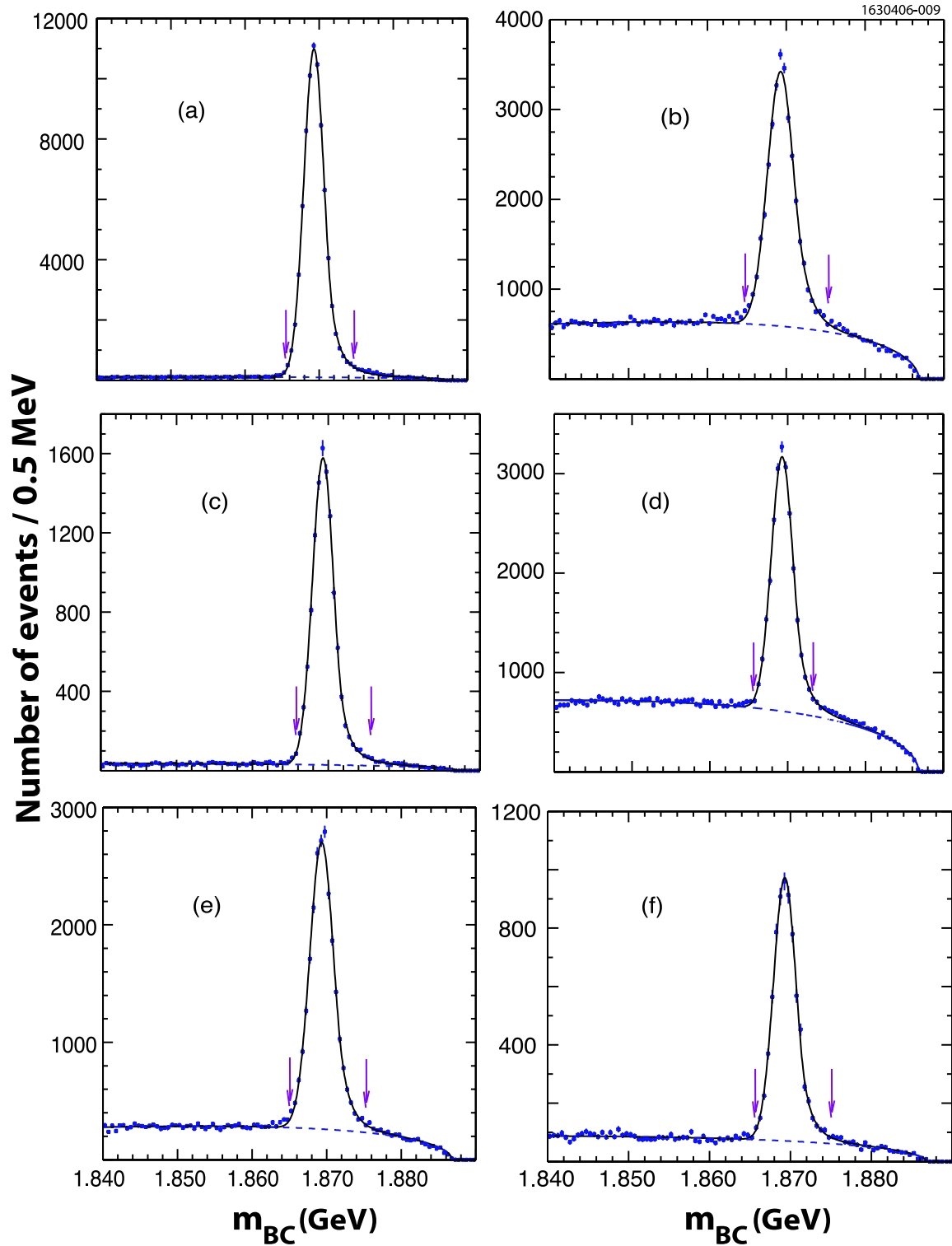


FIG. 2: Beam-constrained mass distributions for different fully reconstructed D^- decay candidates in the final states: (a) $K^+\pi^-\pi^-$, (b) $K^+\pi^-\pi^-\pi^0$, (c) $K_S\pi^-$, (d) $K_S\pi^-\pi^-\pi^+$, (e) $K_S\pi^-\pi^0$ and (f) $K^+K^-\pi^-$. The solid curves show the sum of signal and background functions. The dashed curves indicate the background fits. Events between the arrows are selected for further analysis.

where E_{beam} is the beam energy, E_{track} and $(-\vec{p}_{D^-} - \vec{p}_{track})$ are the measured energy and momentum of a single track, assuming that the track is a pion, and \vec{p}_{D^-} is the three-momentum of the fully reconstructed D^- .

The MM^2 distribution from Monte Carlo simulations of $e^+e^- \rightarrow D^+D^-$, where the D^- is fully reconstructed and $D^+ \rightarrow \tau^+\nu$, $\tau^+ \rightarrow \pi^+\bar{\nu}$, is shown in Fig. 3. While the pion in this decay sequence doesn't have a narrow MM^2 peak as in the case of $D^+ \rightarrow \mu^+\nu$, many events are in the low MM^2 region. The spectrum peaks at low MM^2 because the small $D^+-\tau^+$ mass difference causes the τ^+ to be almost at rest in the laboratory frame and thus the π^+ has relatively large momentum. We must also ensure that we do not accept $D^+ \rightarrow \mu^+\nu$ events or semileptonic decays with electrons.

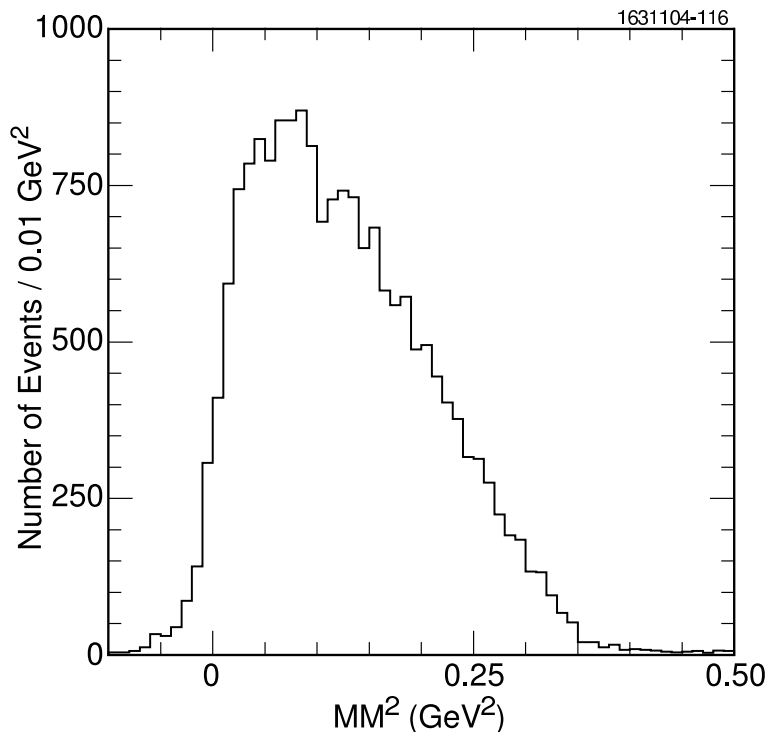


FIG. 3: Missing mass squared distribution for $D^+ \rightarrow \tau^+\nu$, $\tau^+ \rightarrow \pi^+\bar{\nu}$ from Monte Carlo simulation.

Using our D^- event candidates, we search for events with a single additional charged track. The crystal calorimeter provides a way of distinguishing this track among muons, pions and electrons. We consider three separate cases: (i) the track deposits < 300 MeV in the calorimeter, characteristic of a non-interacting pion or a muon; (ii) the track deposits > 300 MeV in the calorimeter, characteristic of an interacting pion; (iii) the track satisfies our electron selection criteria defined below. Then we separately study the MM^2 distributions for these three cases.

We exclude events with more than one additional, opposite-sign charged track in addition to the tagged D , or with extra neutral energy. Specifically, we veto events with extra charged tracks arising from the event vertex or having a maximum neutral energy cluster, consistent with being a photon, of more than 250 MeV. These cuts are highly effective in reducing backgrounds especially from $D^+ \rightarrow \pi^+\pi^0$ decays.

The track candidates are required to be within the barrel region of the detector $|\cos\theta| <$

0.81. For cases (i) and (ii) we insist that the track not be identified as a kaon. For electron identification we require a match between the momentum measurement in the tracking system and the energy deposited in the CsI calorimeter and the shape of the energy distribution among the crystals is consistent with that expected for an electromagnetic shower.

As demonstrated previously [6], the MM^2 distribution has a shape well described by two Gaussians for the $\mu^+\nu$ mode with a resolution from Monte Carlo simulation (MC) of 0.0235 ± 0.0004 GeV². We use different MM^2 regions for cases (i) and (ii) defined above. For case (i) we define the signal region to be the interval $0.175 > MM^2 > 0.05$ GeV², while for case (ii) we define the signal region to be the interval $0.175 > MM^2 > -0.05$ GeV². Case (i) includes 98% of the $\mu^+\nu$ signal, so we must exclude the region close to zero MM^2 , while for case (ii) we are specifically selecting pions so the signal region can be larger. The upper limit on MM^2 is chosen to avoid background from the tail of the $\bar{K}^0\pi^+$ peak. The fractions of the MM^2 range accepted are 46% and 74% for case (i) and (ii), respectively.

The MM^2 distributions for cases (i) and (ii) are shown in Figs. 4 (a) and (b). There are 12 events in the signal region for case (i) and 8 for case (ii). The electron sample, case (iii), shown in Fig. 5, has 3 events in the signal region and is used for background studies.

V. BACKGROUND EVALUATION

A. Monte Carlo Estimates

There are several background sources we need to evaluate. These include background from other D^+ modes, background from misidentified $D^0\bar{D}^0$ events and continuum background including that from $e^+e^- \rightarrow \gamma\psi(2S)$, termed “radiative return.” There are a few D^+ decay modes that have been identified *a priori* as possible background sources. These are listed in Table II, along with the numerical background estimates we obtain using Monte Carlo generation and reconstruction of each specific mode. The branching ratios are from the Particle Data Group except for the $\pi^+\pi^0$ and $\rho^+\pi^0$ modes where we use new CLEO measurements [12]. We note that often at least one photon from the π^0 decay in these two modes exceeds our 250 MeV calorimeter energy requirement and causes these decays to be vetoed.

The $\bar{K}^0\pi^+$ mode gives a large peak in the MM^2 spectrum near 0.25 GeV². We need to evaluate the effects of the tail of the distribution leaking into our signal region. A simulation of this background for case (i) and case (ii) yields $2.4 \pm 0.5 \pm 0.2$, and $1.6 \pm 0.4 \pm 0.1$ events, respectively. The systematic errors are due to uncertainties on the measured branching ratios.

We have also checked the possibility of other D^+D^- decay modes producing background with an equivalent 1.7 fb⁻¹ Monte Carlo sample; we find no additional events. $D^0\bar{D}^0$ and continuum backgrounds are evaluated by analyzing Monte Carlo samples corresponding to 4.7 fb⁻¹ and 1.7 fb⁻¹, respectively. To normalize our Monte Carlo events to our data sample, we used $\sigma_{D^0\bar{D}^0} = 3.6 \pm 0.1$ nb and $\sigma_{\text{continuum}} = 14.5 \pm 1.0$ nb [13]. Our total background is $6.1 \pm 0.6 \pm 0.3$ events in case (i) and $5.0 \pm 0.6 \pm 0.2$ events in case (ii).

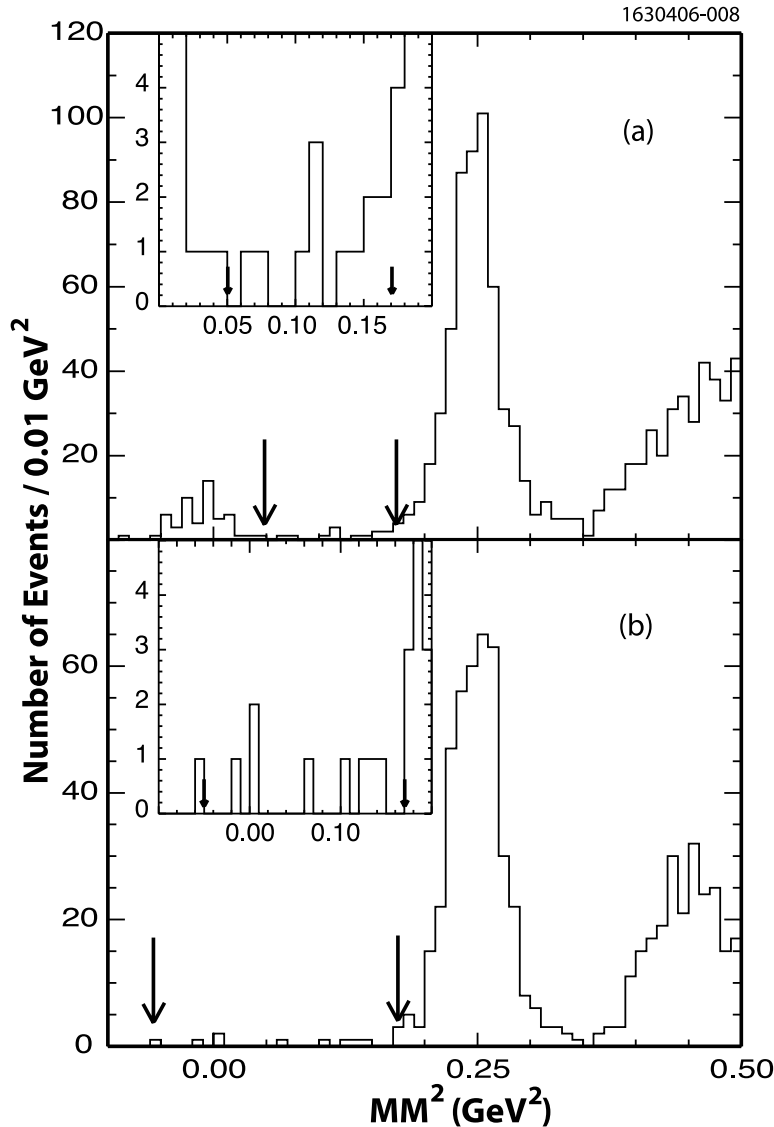


FIG. 4: The MM^2 distributions from data using D^- tags and one additional opposite-sign charged track and no extra energetic showers (see text). For the case when the single track (a) deposits < 300 MeV of energy in the calorimeter, case (i). The peak near zero is from $D^+ \rightarrow \mu^+ \nu$ events. (b) Track deposits > 300 MeV in crystal calorimeter but is not consistent with being an electron, case (ii). The arrows indicate the signal regions. The insets show the signal regions with a finer binning of 0.002 GeV^2 .

B. Background Estimates From Data

The largest source of background is the tail of the $\bar{K}^0 \pi^+$ peak. Simulations of the tails of distributions, however, are often unreliable. Therefore, we also measure this background rate directly from data.

We select $D^0 \bar{D}^0$ events where one neutral D decays into $K^\mp \pi^\pm \pi^+ \pi^-$, $K^\mp \pi^\pm \pi^0$ or $K^\mp \pi^\pm$. These single-tag candidates are reconstructed using tight selection criteria on ΔE and m_{BC} .

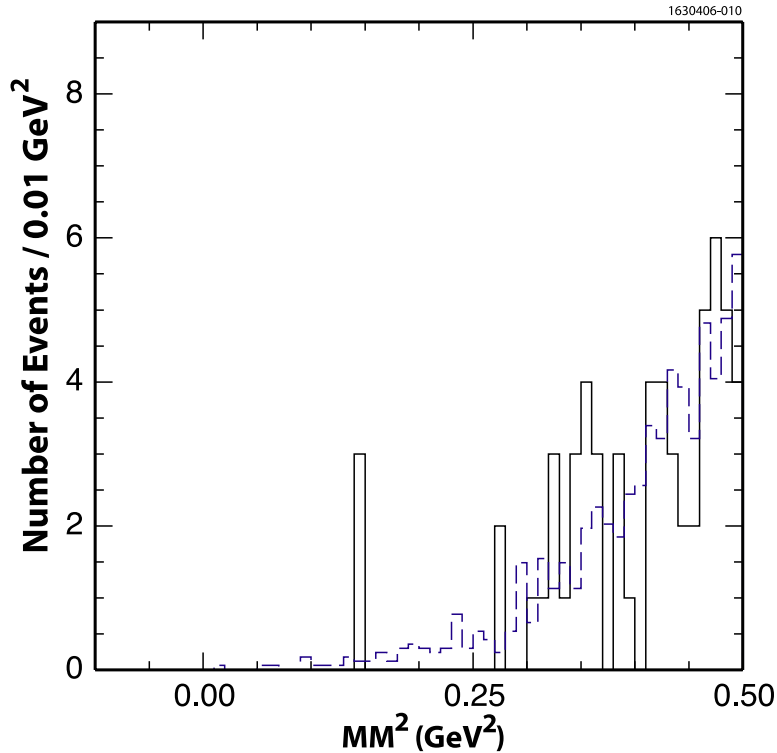


FIG. 5: The MM^2 distribution obtained using D^- tags and one additional opposite-sign charged track and no extra energetic showers (see text). The track is required to deposit > 300 MeV of energy in the calorimeter and be consistent with an electron. The solid curve is data and the dashed curve Monte Carlo.

In this sample, we look for events with only two additional oppositely-signed tracks where the RICH system identifies one as a kaon and the other as a pion. We insist that the charge of the kaon candidate be opposite to the charge of the kaon in the tag mode. Our aim is to isolate the $K^\mp\pi^\pm$ final state opposite the reconstructed tag signal events. We avoid, however, making tight cuts that might ameliorate the effects of tails.

The $K^\mp\pi^\pm$ final state is identical kinematically to the $\bar{K}^0\pi^+$ state that we wish to emulate if we ignore the measurements of the charged kaon and then compute the MM^2 , as shown in Fig. 6 for cases (i) and (ii).

The event numbers in our signal ranges are $4.8 \pm 1.0 \pm 0.1$ for case (i) and $2.5 \pm 0.8 \pm 0.1$ for case (ii). The systematic error arises from the normalization, derived from the fit to the MM^2 peak near 0.25 GeV^2 . There are backgrounds, however, in these distributions from $\bar{D}^0 \rightarrow \pi^+\pi^-$ and $\bar{D}^0 \rightarrow \mu^-\pi^+\bar{\nu}$ events where the candidate kaon is a misidentified pion. The probability for pions faking kaons in this momentum range has been measured as $(1.10 \pm 0.37)\%$ [8]. Using the known branching ratios for the above two modes, we estimate 0.08 and 0.17 $\pi^+\pi^-$ events, respectively, and 0.01 and zero $\pi^+\mu^-\bar{\nu}$ events, respectively, that need to be removed from the background estimate, leaving 4.7 ± 1.0 and 2.4 ± 0.7 background events. This estimate is in reasonable agreement with the simulation. (Since we are going to quote an upper limit in this paper, choosing the Monte Carlo background estimate provides a worse limit because less background is subtracted, and thus is the more conservative choice.)

| Mode | \mathcal{B} (%) | # of events case(i) | # of events case(ii) |
|--|-------------------|---------------------------|---------------------------|
| $\pi^+\pi^0$ | 0.12 ± 0.01 | $0.13\pm 0.02\pm 0.01$ | $1.40\pm 0.07\pm 0.11$ |
| $\overline{K}^0\pi^+$ | 2.77 ± 0.18 | $2.44\pm 0.51\pm 0.17$ | $1.59\pm 0.41\pm 0.11$ |
| $\mu^+\nu$ | 0.04 ± 0.01 | $1.25\pm 0.03\pm 0.19$ | $0.46\pm 0.07\pm 0.07$ |
| $\rho^+\pi^0$ | 0.38 ± 0.03 | $0.18\pm 0.05\pm 0.01$ | $0.23\pm 0.05\pm 0.02$ |
| $\pi^0\mu^+\nu$ | 0.44 ± 0.07 | $0.98\pm 0.14\pm 0.15$ | $0.002\pm 0.001\pm 0.001$ |
| $\tau^+\nu, \tau^+ \rightarrow \rho^+\nu$ | 0.030 ± 0.005 | $0.14\pm 0.01\pm 0.02$ | $0.15\pm 0.01\pm 0.02$ |
| $\tau^+\nu, \tau^+ \rightarrow \mu^+\nu\overline{\nu}$ | 0.020 ± 0.003 | $0.27\pm 0.01\pm 0.04$ | $0.03(32\% \text{ C.L.})$ |
| Other D^+ modes | - | $0.08(32\% \text{ C.L.})$ | $0.08(32\% \text{ C.L.})$ |
| D^0 modes | - | $0.23\pm 0.12\pm 0.01$ | $0.42\pm 0.16\pm 0.01$ |
| Continuum | - | $0.45\pm 0.26\pm 0.03$ | $0.74\pm 0.33\pm 0.05$ |
| Sum | - | $6.07\pm 0.60\pm 0.31$ | $4.99\pm 0.56\pm 0.19$ |

TABLE II: Monte Carlo estimated backgrounds from all sources. The second errors are systematic and are due to uncertainties on the measured branching ratios for D^+ background sources and production cross-section uncertainties for D^0 and continuum sources. The “other D^+ modes listed at 0.08 at 32% c.l. represent a 1σ upper limit on this contribution.

Another background check is to both measure the electron background and simulate it. We note that the background due to real muons should be almost equal to the background due to real electrons. For this study we use the entire MM^2 region up to 0.5 GeV^2 . The MM^2 distribution due to electron candidates in the data is compared with the one from the Monte Carlo in Fig. 5. There are 60 ± 8 electrons in the data compared with 63 ± 3 in the Monte Carlo after normalizing to the luminosity in the data. (In the signal region there are 3 events in the data versus 3.9 ± 0.1 in the Monte Carlo.) The good agreement establishes that the Monte Carlo properly predicts the semileptonic decay backgrounds.

VI. BRANCHING RATIO LIMITS

We do not observe a statistically significant difference between the number of signal and background events. For case (i) we have a net signal of 5.9 $\tau^+\nu, \tau^+ \rightarrow \pi^+\overline{\nu}$ signal events and for case (ii) our yield is 3.0 events. For each of our two cases denoted by j , where j represents either case (i) or case (ii), the expected number of events, N_{expected}^j , is related to the true $\mathcal{B}_{\tau\nu} \equiv \mathcal{B}(D^+ \rightarrow \tau^+\nu)$ through the relationship

$$N_{\text{expected}}^j = N_{\text{tags}} \times \mathcal{B}_{\tau\nu} \times \mathcal{B}(\tau^+ \rightarrow \pi^+\overline{\nu}) \times \varepsilon^j + N_{\text{bkg}}^j, \quad (6)$$

where N_{tags} is the number of single tag events and equals 160,729, after correcting for the slight difference in reconstruction efficiency for tags opposite a single track versus tags opposite a typical D^+ decay; ε^j is the efficiency, and N_{bkg}^j is the background. The Poisson probability distribution $L_j(\mathcal{B}_{\tau\nu})$ for $\mathcal{B}(D^+ \rightarrow \tau^+\nu)$ in each case j has a mean equal to N_{expected}^j and is given by:

$$L_j(\mathcal{B}_{\tau\nu}) = \left(\frac{1}{N_{\text{expected}}^j!} \right) \times \exp\left(-N_{\text{expected}}^j\right) \times \left(N_{\text{expected}}^j\right)^{N_{\text{expected}}^j}, \quad (7)$$

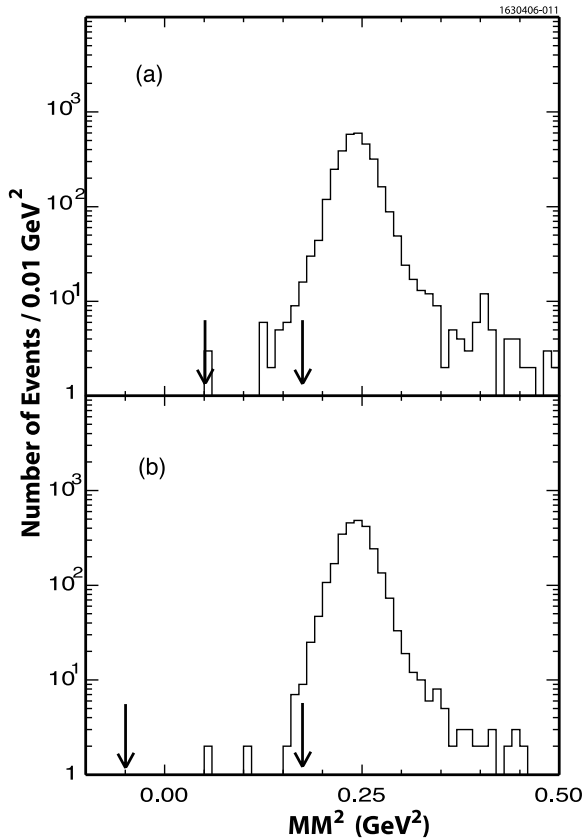


FIG. 6: The MM^2 distribution from data events with a single D^0 or \bar{D}^0 tag and the other neutral D decaying into two tracks, most likely $K^\mp\pi^\pm$, where the kaon information is ignored. For the two cases: (a) track deposits < 300 MeV of energy in the crystal calorimeter and (b) track deposits > 300 MeV in the calorimeter. The arrows delineate the relevant signal regions.

where N^j is the number of detected $\tau^+\nu$ candidates: 8 for case (i) and 12 for case (ii).

Our results for the branching fractions are found by doing a simultaneous likelihood fit of the distributions described in Eq. 7. We take into account the the different efficiencies in cases (i) and (ii) that arises from both the MM^2 acceptance (46% and 74%) and the efficiency of not having another unmatched shower in the event with energy greater than 250 MeV (93.9% and 91.8%). We have previously found [6] that the Monte Carlo matched within 1.8% our measurement of the extra unmatched shower cut and thus use a slightly larger 2% for the systematic error on this quantity. Overall, the efficiencies are 18.7% (22.4%), for case (i) and (case(ii)), respectively.

We find $\mathcal{B}(D^+ \rightarrow \tau^+\nu) = (1.8_{-0.9}^{+1.2} \pm 0.1) \times 10^{-3}$ and $(0.8_{-0.5}^{+0.9} \pm 0.2) \times 10^{-3}$, for cases (i) and (ii), respectively, where the statistical errors result from the values of $\mathcal{B}_{\tau\nu}$ corresponding to 34% of the area under the L_J distribution above and below the maximum value.

The errors on the backgrounds are treated as systematic and are obtained by varying the background contributions in the likelihood distribution. The systematic errors on the branching ratio from sources other than backgrounds are listed in Table III; they are negligible in comparison with the statistical uncertainty. A more detailed explanation of the sources of systematic errors can be found in our previous Letter [6].

| | Systematic errors (%) |
|------------------------|-----------------------|
| MC statistics | 0.2 |
| Track finding | 0.7 |
| PID cut | 1.0 |
| Minimum ionization cut | 1.0 |
| Number of tags | 0.5 |
| Extra showers cut | 2.0 |
| Total | 2.6 |

TABLE III: Systematic errors on the $D^+ \rightarrow \tau^+\nu_\tau$ branching ratio.

To obtain a combined result for the branching fraction, we construct the global likelihood as the product of the two Poisson probability distributions, and we extract the value of $\mathcal{B}_{\tau\nu}$ which maximizes this likelihood function. We find $\mathcal{B}(D^+ \rightarrow \tau^+\nu) = (1.2_{-0.6}^{+0.7} \pm 0.1) \times 10^{-3}$. We caution the reader that this is not a definitive measurement but an intermediate step used in the process of forming an upper limit. (Had we used the data to estimate the background, the branching fraction would be lower.)

Since the result is not statistically significant we quote an upper limit of

$$\mathcal{B}(D^+ \rightarrow \tau^+\nu) < 2.1 \times 10^{-3} \quad (8)$$

at 90% confidence level.

The ratio to the expected rate in the Standard Model using our measured $\mathcal{B}(D^+ \rightarrow \mu^+\nu)$ is < 1.8 at 90% confidence level.

VII. CONCLUSIONS

We have measured the first upper limit on the decay $D^+ \rightarrow \tau^+\nu$. We limit $\mathcal{B}(D^+ \rightarrow \tau^+\nu)$ branching ratio to $< 2.1 \times 10^{-3}$ at 90% confidence level. We use our previously measured result of $\mathcal{B}(D^+ \rightarrow \mu^+\nu_\mu) = (4.40 \pm 0.66_{-0.12}^{+0.09}) \times 10^{-4}$, [6], coupled with the evaluation of Eq. (2) of 2.65, to limit the ratio $R = \Gamma(D^+ \rightarrow \tau^+\nu) / \Gamma(D^+ \rightarrow \mu^+\nu)$ to that expected in the Standard Model to < 1.8 at 90% confidence level. Thus lepton universality in purely leptonic D^+ decays is satisfied at the level of current experimental accuracy.

VIII. ACKNOWLEDGMENTS

We gratefully acknowledge the effort of the CESR staff in providing us with excellent luminosity and running conditions. We thank K. Agashe for useful discussions. D. Cronin-Hennessy and A. Ryd thank the A.P. Sloan Foundation. This work was supported by the National Science Foundation, the U.S. Department of Energy, and the Natural Sciences and

- [1] D. Silverman and H. Yao, Phys. Rev. D **38**, 214 (1988).
- [2] We assume that $|V_{cd}|$ equals $|V_{us}|$ and take the value from the average given by Nierste, “Quark mixing and CP violation - the CKM matrix,” [hep-ph/0511125].
- [3] J. Hewett, “Seaching For New Physics with Charm,” SLAC-PUB-95-6821 (2005) [hep-ph/9505246].
- [4] W.-S. Hou, Phys. Rev. D **48**, 2342 (1993).
- [5] S. Eidelman *et al.* (PDG), Phys. Lett. B **592**, 1 (2004).
- [6] M. Artuso *et al.* (CLEO Collaboration), Phys. Rev. Lett. **95**, 251801 (2005) [hep-ex/0508057].
- [7] D. Peterson *et al.*, Nucl. Instrum. and Meth. **A478**, 142 (2002); M. Artuso *et al.*, Nucl. Instrum. and Meth. **A502**, 91 (2003); Y. Kubota *et al.* (CLEO Collaboration), Nucl. Instrum. and Meth. **A320**, 66 (1992).
- [8] M. Artuso *et al.*, Nucl. Instrum. Meth. **A554**, 147 (2005) [physics/0506132].
- [9] G. Bonvicini *et al.* (CLEO Collaboration), Phys. Rev. **D70**, 112004 (2004) [hep-ex/0411050].
- [10] The function is $f(m_{BC}) = A(m_{BC} + B)\sqrt{1 - \left(\frac{m_{BC}+B}{C}\right)^2} \exp\left[D\left(1 - \left[\frac{m_{BC}+B}{C}\right]^2\right)\right]$. Here A is the overall normalization and B , C and D are parameters that govern the shape. See H. Albrecht *et al.* (ARGUS Collaboration), Phys. Lett. B **229**, 304 (1989).
- [11] T. Skwarnicki, “A Study of the Radiative Cascade Transitions Between the Upsilon-Prime and Upsilon Resonances,” DESY F31-86-02 (thesis, unpublished) (1986).
- [12] P. Rubin *et al.* (CLEO Collaboration), Phys. Rev. Lett. **96**, 081802 (2006) [hep-ex/0512063].
- [13] Q. He *et al.* (CLEO Collaboration), Phys. Rev. Lett **95**, 121801 (2005) [hep-ex/0504003].